[redacted]

CONFIDENTIAL

Copy
RM L[redacted]

TECH LIBRARY KAFB, NM
0144804

5823

NACA RM L57G29

7799

RESEARCH MEMORANDUM

FREE-FLIGHT INVESTIGATION OF THE DRAG OF A MODEL OF A 60° DELTA-WING BOMBER WITH STRUT-MOUNTED SIAMESE NACELLES AND INDENTED FUSELAGE AT MACH NUMBERS FROM 0.80 TO 1.35

By Sherwood Hoffman

Langley Aeronautical Laboratory
Langley Field, Va.

[redacted]

NATIONAL ADVISORY COMMITTEE
FOR AERONAUTICS
WASHINGTON
September 25, 1957

CONFIDENTIAL

[redacted]

TECH LIBRARY KAFB, NM
0144804

[redacted]

NATIONAL ADVISORY COMMITTEE FOR AERONAUTICS

RESEARCH MEMORANDUM

FREE-FLIGHT INVESTIGATION OF THE DRAG OF A MODEL OF A 60° DELTA-WING BOMBER WITH STRUT-MOUNTED SIAMESE NACELLES AND INDENTED FUSELAGE AT MACH NUMBERS FROM 0.80 TO 1.35

By Sherwood Hoffman

SUMMARY

A model of a 60° delta-wing bomber with strut-mounted Siamese nacelles was designed, with the use of a symmetrical fuselage indentation, to have a smooth average area distribution at a Mach number of 1.20. The nacelles were mounted on 70° sweptforward pylons and had a fineness ratio of 8.9. The flight test covered a range of Mach number from 0.80 to 1.35 and Reynolds number from about 10×10^6 to 20×10^6. Also tested were isolated nacelles, several equivalent bodies of revolution, and a symmetrical configuration with equivalent bodies replacing the nacelle-strut combination.

The results show that the configuration drag rise was significantly higher than that from the equivalent-body tests and area-rule theory throughout the Mach number range. The comparisons make it evident that the equivalent-body concept, used in either theory or experiment, may not account for all the interference effects, especially local interference.

Near a Mach number of 1.20, the drag rise of the configuration was equal to that of a similar bomber with staggered individual nacelles, which was designed for a Mach number of 1.00. The drag rise was somewhat higher at transonic speeds.

INTRODUCTION

This paper presents the results of an application of the supersonic area rule (ref. 1) to the design of a 60° delta-wing bomber with strut-mounted Siamese nacelles. The nacelles were mounted below the wing on

[redacted]

[redacted]

70° sweptforward pylons. The area distribution of a parabolic body of fineness ratio 8 and a Mach number of 1.2 were chosen as the design conditions. The fuselage was indented symmetrically to cancel the average of the projected areas at all angles of roll intercepted by inclined Mach planes of the wing, nacelles, struts, and fins. It should be noted that the symmetrical fuselage indentation is not optimum for this case since the nacelles are mounted below the wing. According to reference 2, radial body contouring as well as axial body contouring would be required to minimize the pressure drag. Aspects of the area rule were investigated also by substituting equivalent bodies of revolution for the Siamese nacelle-strut combinations and mounting them like large symmetrical stores on the wing, by computing the configuration pressure drag with the use of area-rule theory, and by tests of equivalent bodies for the configuration and isolated Siamese nacelles. In addition, small models of the Siamese nacelles and a single nacelle were tested to determine the interference between the nacelles.

The configurations were rocket-propelled vehicles tested through a range of Mach number from 0.80 to 1.35 and Reynolds numbers, based on wing mean aerodynamic chord, from 10×10^6 to 20×10^6.

SYMBOLS

A	cross-sectional area, sq ft
a	longitudinal acceleration, ft/sec^2
C_D	total drag coefficient, based on S_W
C_{D_N}	nacelle drag coefficient, based on S_N
C_{D_f}	friction drag coefficient, based on S_W or S_N
ΔC_D	drag rise or pressure drag coefficient, based on S_W
ΔC_{D_N}	drag rise or pressure drag coefficient, based on S_N
g	acceleration due to gravity, 32.2 ft/sec^2
L	length of fuselage, ft
l	length of nacelle, ft

[redacted]

M	free-stream Mach number
q	free-stream dynamic pressure, lb/sq ft
R	Reynolds number, based on wing mean aerodynamic chord
S_W	total wing plan-form area, sq ft
S_N	frontal area of single nacelle, sq ft
W	weight, lb
x	station measured from nacelle nose, ft
X	station measured from fuselage nose, ft
γ	elevation angle of flight path, deg
ϕ	roll angle, deg

$\beta = \sqrt{M^2 - 1}$

MODELS

Details and dimensions of the models tested are given in figure 1 and tables I to VIII. The cross-sectional area distributions and photographs of the models are shown in figures 2 and 3, respectively.

The wing-body configuration with the strut-mounted Siamese nacelles (model A) was designed to have a smooth average area distribution at Mach number 1.20 (fig. 2(b)). The 60° delta wing used had an aspect ratio of 2.096, an NACA 65A004 airfoil section in the free-stream direction, 10° forward sweep for the trailing edge, and was alined with the center line of the fuselage. The pointed wing tip was modified with a small radius. The quarter-chord point of the mean aerodynamic chord was located longitudinally at a station corresponding to the 60-percent station of the fuselage. The ratio of total wing plan-form area to fuselage frontal area was 31.2.

Each nacelle had a design mass-flow ratio of 1.0, a sharp lip for the inlet and exit, a cylindrical duct, and an overall fineness ratio of 8.9. The nacelle length was 0.821 of the wing mean aerodynamic chord. The ratio of total nacelle frontal area to total wing plan-form area was about 0.0225. There was no incidence between the nacelle, wing, and fuselage.

[redacted]

The pylons had 70° of sweepforward from the wing leading edge at the 0.456-semispan station, an NACA 65A006 airfoil section in the stream direction, no taper, and a chord length equal to 0.535 of the wing mean aerodynamic chord. No fillets were employed at any of the junctures of the components of the configuration.

The configuration (model A) included two 60° sweptback vertical stabilizing fins as shown in figure 1(a). Geometrically similar fins were used on all the models tested.

For the present design application, the cross-sectional area distribution of a parabolic body of revolution of fineness ratio 8 (table V) was selected for the desired average area distribution at Mach number 1.20. The areas used for indenting this body were obtained from the average of the frontal projection of the exposed wing areas, nacelle areas, pylon areas, and fin areas cut by Mach planes at $M = 1.20$ for all angles of roll (ϕ) of the Mach planes with respect to the configuration. These average areas were obtained by using Faget's rapid "method of hoops" (ref. 3). The nacelle inlet area was subtracted from the nacelle total cross-sectional area to allow for internal flow. The wing and fin areas which intercepted the fuselage axis downstream of the fuselage base were neglected. The fuselage fineness ratio after indenting was 10.067.

Model B was identical to model A except for the nacelles and pylons. For this model (model B), each pair of nacelles and pylon was replaced by its Mach number 1.0 equivalent body of revolution and mounted symmetrically about the wing (fig. 1(c)). The normal cross-sectional area of the equivalent body was adjusted to allow for the cross-sectional areas of the wing covered by the body.

Model C was the Mach number 1.0 equivalent body of revolution of models A and B. Model D corresponded to the average equivalent body for either models A or B at the design Mach number of 1.2. The area distributions of these bodies were altered to compensate for the additional areas due to their stabilizing fins.

Models E and F were duplicate models of one pair of nacelles or Siamese nacelle, model G was the Mach number 1.0 equivalent body of revolution for the Siamese nacelle, and model H was a model of a single nacelle. Because of the sharp lip at the exit of the nacelles (models E, F, and H), it was necessary to cut off the rear 4.2-percent length of the nacelles to obtain sufficient bearing area for boosting (propelling the models from the helium gun).

[redacted]

TEST TECHNIQUE

All the models were tested at the Langley Pilotless Aircraft Research Station at Wallops Island, Va. The two wing-body nacelle configurations, models A and B, were boosted to supersonic speeds by fin-stabilized 6-inch ABL Deacon rocket motors. Model A and booster in launching position are shown in figure 3(j). After burnout of the booster rocket fuel, the higher drag-weight ratio of the booster, as compared with that of the model, allowed the model to separate longitudinally from the booster. The small models C, D, E, F, G, and H were propelled to supersonic speeds from a helium gun which is described in reference 4. Velocity and trajectory data were obtained from the CW Doppler velocimeter and the NACA modified SCR-584 tracking radar unit, respectively. A survey of atmospheric conditions including winds aloft was made from an ascending balloon that was released at the time of each launching.

DATA REDUCTION AND ANALYSIS

The total drag coefficient of each model was determined during decelerating or coasting flight. For models A and B, C_D was evaluated from the expression

$$C_D = -\frac{W}{gqS_W}\left[a + g \sin \gamma\right]$$

where a was obtained by differentiating the velocity-time curve from Doppler radar. The values of q and γ were obtained from the measurements of tangential velocity and atmospheric conditions along the trajectory of each model. The drag coefficients of the equivalent-body models (C and D) were determined in the same manner as for models A and B but were based on scaled-down S_W. Similarly, C_{D_N} for the Siamese nacelle models (models E and F) and their equivalent body of revolution (model G) was based on the total frontal area $2S_N$ of one Siamese nacelle arrangement. The drag coefficient of the single nacelle, model H, was based on its frontal area S_N.

The error in total drag coefficient, based on S_W, was estimated to be less than ±0.0007 at supersonic speeds and ±0.001 at subsonic speeds. The Mach numbers were determined within ±0.01 throughout the test range.

The drag-rise coefficient, or experimental pressure drag coefficient, was obtained by subtracting an estimated friction drag C_{D_f} and, when

required, the nacelle internal pressure drag from the total drag at corresponding Mach numbers. The friction-drag variation through the Mach number range was determined by adjusting the subsonic drag level of each model for Reynolds number effect with use of the equations of Van Driest (ref. 5). For the variations of skin friction with Reynolds number, it was assumed that the boundary layer over the fuselage, bodies, and nacelles was altogether turbulent and that transition was at the 30-percent- and 50-percent-chord stations of the smooth metal delta wings and fins, respectively.

The nacelle internal pressure drag was estimated by computing the momentum loss for the entering stream tube with the assumption of a normal shock at the inlet and a mass-flow ratio of 1.0. No adjustments were made for the base-drag rise of any of the models. References 6 and 7 indicate that, for afterbodies similar to those used herein, the base drag rise is small and of the order of accuracy of the drag measurements.

The theoretical pressure drags were computed for the two wing-body-nacelle configurations, models A and B, by using the supersonic area rule of reference 1. The computational procedure is described in references 8 and 9. For model A, which was unsymmetrical in that the Siamese nacelles were mounted below the wing, it was necessary to determine the longitudinal distribution of the frontal projection of oblique areas cut by inclined Mach planes between roll angles of 0° and 180°. The area distributions obtained corresponded to values of $\beta \cos \phi$ equal to 0, ±0.250, ±0.500, ±0.750, and ±1.118. Model B was symmetrical and only the areas between 0° and 90° of roll (positive values of $\beta \cos \phi$) had to be considered.

Since the fuselage was fairly slender (fineness ratio 10.067), it was possible to simplify the calculations by using the normal area distribution of the fuselage in combination with the oblique area distributions of the wing, struts, and nacelles. As another simplification, the area distributions of the thin sweptback fins were neglected. Also, it has been assumed for the calculations that a cylinder can be added at the base of the body without altering the drag. If this assumption were not made, the solution would require the flow to fill the area behind the base and would exceed the limitations of the linearized theory. All the area distributions and their slopes were obtained graphically. (See ref. 10.)

The Fourier sine series used for calculating the pressure drag were evaluated for 66 harmonics and plots of these series indicated that they were convergent.

RESULTS AND DISCUSSION

The rocket-propelled models, A and B, were tested through a range of Mach number from 0.80 to about 1.35 with corresponding Reynolds number from about 10×10^6 to 20×10^6. The small models (C to H), which were propelled from the helium gun, covered a Mach number range from about 0.8 to 1.3 with corresponding Reynolds numbers from approximately 4×10^6 to 7×10^6. The Reynolds numbers are presented in figure 4 and are based on wing mean aerodynamic chord adjusted for model scale.

Total Drag

The basic drag data for the models are presented in figures 5 and 6. The solid curves are fairings through the measured total drag coefficients. The dashed curves marked C_{D_f} show the variations of friction drag coefficient (including subsonic interference) through the Mach number and Reynolds number ranges of the tests. All the models were flight tested at zero-lift or near zero-lift conditions. Model A, which was unsymmetrical, was ballasted to give a static margin approximately equal to one mean aerodynamic chord length. This condition resulted in very low trim lift coefficients for which the induced drag is negligible (see, for example, ref. 11).

The nacelle external drag coefficient for models E, F, and H, as shown in figure 6, were determined by subtracting the computed internal drag coefficient and the drag of the stabilizing fins (ref. 7) from the total drag coefficient. The external drag coefficient shown for the Siamese nacelles is the average external drag of models E and F. The single nacelle, model H, was lost by the Doppler radar during the test and data were obtained only between Mach numbers of 1.16 and 1.31.

Figure 7 presents a comparison of the total drag coefficients of the wing-body-nacelle configurations and the external drag coefficients (based on S_w) of two pairs of Siamese nacelles and four single nacelles. The drag coefficient of model A is appreciably higher than that of model B throughout the test range. The difference in C_D between models A and B at $M = 0.8$ is due largely to the difference in skin friction for the configurations. At $M = 1.35$, the configuration with the strut-mounted nacelles had about 40 percent more drag than the configuration with the equivalent nacelle installation.

The drag of two Siamese nacelles at high subsonic speeds is approximately equal to 40 percent of the configuration drag. Although the isolated nacelle models were smaller than those used on model A, their

values of drag coefficient are as valid as those for the larger nacelles. The difference in friction drag coefficient due to the difference in test Reynolds number is less than the accuracy of measurements. The increment in C_D between model A and the Siamese nacelles near $M = 0.9$ is of the order of magnitude of C_D for similar 60° delta-wing configurations without nacelles in reference 7.

Figure 7 also shows that the isolated Siamese nacelles had nearly 50 percent more drag than the corresponding number of single nacelles near Mach number 1.2. Since the friction drag and internal drag coefficients are the same for the nacelle models, this difference is due to unfavorable pressure interference between the nacelles of the Siamese nacelle arrangement.

Pressure Drag

A comparison of the values of drag rise for the two configurations, their equivalent bodies of revolution, and the theoretical pressure drag is presented in figure 8. Only one theoretical curve is shown since the theory gave approximately the same values of ΔC_D for each configuration. The graphically determined area distributions and slopes for models A and B were so nearly the same that only a negligible effect of nacelle vertical displacement on the theoretical drag was obtained. Also, for the comparison, the average drag rise of models C and D was used in an attempt to estimate the configuration drag rise at $M = 1.2$. Model C corresponds to the area distribution at $\beta \cos \phi = 0$ for $M = 1.2$ as well as the normal area distribution at $M = 1.0$. Model D, or the average-area body, is also an equivalent body at $M = 1.2$ (the value of $\beta \cos \phi$ for this case has not been determined). According to the supersonic area rule (ref. 1) the average drag rise of these bodies should give a rough approximation of the configuration drag rise.

The results in figure 8 show that the configuration with the strut-mounted nacelles had significantly more pressure drag (drag rise) than the equivalent-area models, as well as more than theory would predict, throughout the Mach number range. At Mach number 1.0, for instance, where models A, B, and C had identical nondimensional area distributions, the drag rise of model A is about 26 percent higher than that from model B and 49 percent higher than that from model C. In a similar investigation, reference 12, approximately the same discrepancy in ΔC_D was obtained between a sweptback-wing configuration with underwing stores and its equivalent-area model. Although models A and B had essentially the same area distributions throughout the Mach number range, a substantial difference in ΔC_D was obtained. This difference is due to the

different nacelles and their interference with the wing and fuselage. It is evident that the equivalent-body concept, used in either the linearized area-rule theory or experiment, does not account for all the interference effects, especially local interference. The fairly good agreement in ΔC_D for model B, the equivalent bodies, and the theory appears to be due to low interference drag between the components of the symmetrical configuration. By moving the nacelles from the underslung to the symmetrical position, the local interference between the nacelles and wing was reduced and the symmetrical fuselage indentation became more effective in canceling the interference pressures from the nacelles.

It is of interest to compare the present $M = 1.2$ design with the $M = 1.0$ design of a similar configuration from reference 13. The referenced model had staggered individual nacelles, an equivalent body of fineness ratio 9.0, and a smaller volume for a given fuselage length than model A as is shown in figure 9. Also, the data obtained from this reference were adjusted herein to account for the variation of skin friction drag coefficient with Reynolds number (see fig. 4) through its Mach number range. A comparison of the drag rises and normal area distributions, on the basis of the transonic area rule of reference 14, in figure 9 shows that near $M = 1.0$ model A has the higher ΔC_D and a poorer area distribution. Near $M = 1.2$, the drag rise of model A and that of the model of reference 13 are equal. Also shown for comparison are the drag-rise test points and normal area distribution of a bomber-type airplane from reference 15.

Figure 10 shows a comparison of the values of drag rise of the Siamese nacelles and their Mach number 1.0 equivalent body of revolution. The solid curve is the average (external) drag rise of the Siamese nacelle models E and F. The drag rise of the equivalent body (model G) was 15 percent lower than ΔC_{D_N} for the Siamese nacelles at $M = 1.0$ and 10 percent lower at $M = 1.2$. Reference 16 shows approximately the same agreement between a sharp-lipped single nacelle and its equivalent body near Mach number 1.0.

CONCLUDING REMARKS

For the present investigation, the area rule was used to design a model of a 60° delta-wing bomber with strut-mounted Siamese nacelles for a Mach number of 1.20 and to make predictions of the drag rise up to a Mach number of 1.40. The results show that the configuration drag rise was significantly higher than those from equivalent body tests and supersonic area-rule theory throughout the Mach number range. The comparisons

and referenced data make it evident that the equivalent-body concept, used in either theory or experiment, may not account for all the interference effects, especially local interference.

Near a Mach number of 1.2, the drag rise of the present configuration was equal to that of a similar bomber with staggered individual nacelles, which was designed for a Mach number of 1.0. The drag rise was somewhat higher at transonic speeds.

Langley Aeronautical Laboratory,
National Advisory Committee for Aeronautics,
Langley Field, Va., July 11, 1957.

REFERENCES

1. Jones, Robert T.: Theory of Wing-Body Drag at Supersonic Speeds. NACA Rep. 1284, 1956. (Supersedes NACA RM A53H18a.)

2. Lomax, Harvard, and Heaslet, Max. A.: A Special Method for Finding Body Distortions That Reduce the Wave Drag of Wing and Body Combinations at Supersonic Speeds. NACA RM A55B16, 1955.

3. Hoffman, Sherwood, Wolff, Austin L., and Faget, Maxime A.: Flight Investigation of the Supersonic Area Rule for a Straight Wing-Body Configuration at Mach Numbers Between 0.8 and 1.5. NACA RM L55C09, 1955.

4. Hall, James Rudyard: Comparison of Free-Flight Measurements of the Zero-Lift Drag Rise of Six Airplane Configurations and Their Equivalent Bodies of Revolution at Transonic Speeds. NACA RM L53J21a, 1954.

5. Van Driest, E. R.: Turbulent Boundary Layer in Compressible Fluids. Jour. Aero. Sci., vol. 18, no. 3, Mar. 1951, pp. 145-160, 216.

6. Falanga, Ralph A.: A Free-Flight Investigation of the Effects of Simulated Sonic Turbojet Exhaust on the Drag of a Boattail Body With Variable Jet Sizes From Mach Number 0.87 to 1.50. NACA RM L55F09a, 1955.

7. Morrow, John D., and Nelson, Robert L.: Large-Scale Flight Measurements of Zero-Lift Drag of 10 Wing-Body Configurations at Mach Numbers From 0.8 to 1.6. NACA RM L52D18a, 1953.

8. Holdaway, George H.: Comparison of the Theoretical and Experimental Zero-Lift Drag-Rise Characteristics of Wing-Body-Tail Combinations Near the Speed of Sound. NACA RM A53H17, 1953.

9. Alksne, Alberta: A Comparison of Two Methods for Computing the Wave Drag of Wing-Body Configurations. NACA RM A55A06a, 1955.

10. Nelson, Robert L., and Welsh, Clement J.: Some Examples of the Applications of the Transonic and Supersonic Area Rules to the Prediction of Wave Drag. NACA RM L56D11, 1956.

11. Jacobsen, Carl R.: Effects of Spanwise, Chordwise, and Vertical Location of an External Store on the Aerodynamic Characteristics of a 60° Delta Wing at Mach Numbers of 1.41, 1.62, and 1.96. NACA RM L52H29, 1952.

12. Hall, James Rudyard: Two Experiments on Applications of the Transonic Area Rule to Asymmetric Configurations. NACA RM L56A25, 1956.

13. Hopko, Russell N., Piland, Robert O., and Hall, James R.: Drag Measurements at Low Lift of a Four-Nacelle Airplane Configuration Having a Longitudinal Distribution of Cross-Sectional Area Conducive to Low Transonic Drag Rise. NACA RM L53E29, 1953.

14. Whitcomb, Richard T.: A Study of the Zero-Lift Drag-Rise Characteristics of Wing-Body Combinations Near the Speed of Sound. NACA Rep. 1273, 1956. (Supersedes NACA RM L52H08.)

15. Petersen, Robert B.: Comparison of Experimental and Theoretical Zero-Lift Wave-Drag Results for Various Wing-Body-Tail Combinations at Mach Numbers Up to 1.9. NACA RM A56I07, 1957.

16. Walters, Richard E.: Application of Transonic Area Rule to a Sharp-Lipped Ducted Nacelle. NACA RM L53J09b, 1954.

TABLE I.- COORDINATES OF FUSELAGE (MODELS A AND B)

[Stations measured from body nose]

Station, in.	Ordinate, in.
0	0
.10	.021
.20	.042
.50	.103
1.00	.205
3.00	.599
5.00	.969
7.00	1.317
9.00	1.641
11.00	1.942
13.00	2.219
15.00	2.474
17.00	2.705
19.00	2.870
21.00	2.960
23.00	2.980
25.00	2.970
27.00	2.890
29.00	2.740
31.00	2.520
33.00	2.240
35.00	2.050
37.00	1.950
39.00	1.900
41.00	1.890
43.00	1.890
45.00	1.950
47.00	2.040
49.00	2.090
51.00	2.080
53.00	2.005
55.00	1.850
57.00	1.682
59.00	1.500
60.00	1.400

TABLE II.- COORDINATES OF NACA 65A004 AIRFOIL

OF WINGS (MODELS A AND B)

[Stations measured from leading edge]

Station, percent chord	Ordinate, percent chord
0	0
.5	.311
.75	.378
1.25	.481
2.5	.656
5.0	.877
7.5	1.062
10.0	1.216
15.0	1.463
20.0	1.649
25.0	1.790
30.0	1.894
35.0	1.962
40.0	1.996
45.0	1.996
50.0	1.952
55.0	1.867
60.0	1.742
65.0	1.584
70.0	1.400
75.0	1.193
80.0	.966
85.0	.728
90.0	.490
95.0	.249
100.0	.009

L.E. radius: 0.102 percent chord
T.E. radius: 0.010 percent chord

TABLE III.- COORDINATES OF NACA 65A006 AIRFOIL

OF STRUTS (MODEL A)

[Stations measured from leading edge]

Station, percent chord	Ordinate, percent chord
0	0
.5	.464
.75	.563
1.25	.718
2.5	.981
5.0	1.313
7.5	1.591
10.0	1.824
15.0	2.194
20.0	2.474
25.0	2.687
30.0	2.842
35.0	2.945
40.0	2.996
45.0	2.992
50.0	2.925
55.0	2.793
60.0	2.602
65.0	2.364
70.0	2.087
75.0	1.775
80.0	1.437
85.0	1.083
90.0	.727
95.0	.370
100.0	.013

L.E. radius: 0.229 percent chord
T.E. radius: 0.014 percent chord

TABLE IV.- COORDINATES OF MACH NUMBER 1.0 EQUIVALENT BODY

(MODEL C) OF WING-BODY-NACELLE-STRUT CONFIGURATIONS[a]

[Stations measured from body nose]

Station, in.	Ordinate, in.
0	0
.017	.0035
.033	.0070
.083	.0172
.167	.0342
.500	.0999
.834	.1615
1.167	.2195
1.500	.2735
1.834	.3237
2.167	.3699
2.500	.4124
2.834	.4509
3.167	.4780
3.501	.4930
3.834	.5000
4.168	.5401
4.501	.5901
4.834	.6220
5.168	.6251
5.501	.6251
5.835	.6318
6.168	.6385
6.501	.6451
6.835	.6335
7.168	.6068
7.501	.5734
7.835	.5501
8.168	.5351
8.502	.5068
8.835	.4584
9.168	.3200
9.502	.2717
9.835	.2714
10.000	.2234

[a]The ordinates have been adjusted to correct the body areas for the cross-sectional area distribution of the stabilizing fins used for this equivalent body.

[redacted]

TABLE V.- COORDINATES OF MACH NUMBER 1.2 AVERAGE EQUIVALENT BODY (MODEL D) OF WING-BODY-NACELLE-STRUT CONFIGURATIONS[a]

[Stations measured from body nose]

Station, in.	Ordinate, in.
0	0
.017	.0035
.033	.0070
.083	.0172
.167	.0342
.500	.0999
.834	.1615
1.167	.2195
1.500	.2735
1.834	.3237
2.167	.3699
2.500	.4124
2.834	.4509
3.167	.4858
3.501	.5166
3.834	.5436
4.168	.5668
4.501	.5861
4.834	.6013
5.168	.6131
5.501	.6208
5.835	.6246
6.168	.6245
6.501	.6196
6.835	.6098
7.168	.5950
7.501	.5753
7.835	.5496
8.168	.5183
8.502	.4794
8.835	.4358
9.168	.3842
9.502	.3324
9.835	.2812
10.000	.2545

[a]The ordinates have been adjusted to correct the body areas for the cross-sectional area distribution of the stabilizing fins used for this equivalent body.

TABLE VI.- COORDINATES OF DUCTED NACELLE[a] OF THE WING-BODY-NACELLE-STRUT CONFIGURATION (MODEL A)

[Stations measured from nacelle nose]

Station, in.	Ordinate, in.
0	0.720
.250	.747
.500	.777
.750	.809
.950	.833
1.150	.861
1.350	.887
1.550	.921
1.750	.937
2.150	.985
2.950	1.074
3.750	1.160
4.263	1.206
4.905	1.240
5.462	1.250
↓	↓
13.879	1.250
14.199	1.249
15.482	1.231
16.122	1.213
17.405	1.157
18.687	1.077
19.968	.971
20.610	.910
21.316	.834
22.250	.720
Inside diameter = 0.720 in.	

[a]Coordinates of the isolated nacelle models tested (models E, F, and H) are 0.449 scale of those shown in the table.

TABLE VII.- COORDINATES OF MACH NUMBER 1.0 EQUIVALENT

BODY OF SIAMESE NACELLE (MODEL G)

[Stations measured from nacelle nose]

Station, in.	Ordinate, in.
0	0
.112	.126
.225	.184
.337	.229
.427	.268
.517	.302
.607	.331
.697	.358
.787	.384
.966	.426
1.146	.470
1.326	.508
1.506	.545
1.685	.579
1.865	.608
1.916	.615
2.060	.631
2.204	.642
2.348	.649
2.455	.650
↓	↓
6.382	.650
6.525	.648
6.715	.645
6.958	.635
7.246	.621
7.534	.602
7.822	.577
8.110	.545
8.398	.510
8.687	.466
8.974	.416
9.119	.386
9.263	.352
9.407	.319
9.580	.270
9.775	.192
10.000	0

TABLE VIII.- COORDINATES OF THE MACH NUMBER 1.0 EQUIVALENT BODY OF THE SIAMESE NACELLE-STRUT COMBINATION (MODEL B)[a]

[Stations measured from nacelle nose]

Station, in.	Ordinate, in.
0	0
.250	.180
.500	.375
.750	.511
1.150	.672
1.750	.852
2.750	1.091
3.750	1.287
4.750	1.425
5.750	1.492
6.750	1.520
7.750	1.557
8.750	1.605
9.750	1.659
10.750	1.708
11.750	1.749
12.750	1.782
13.750	1.803
14.750	1.814
15.750	1.795
16.750	1.724
17.750	1.609
18.750	1.462
19.750	1.296
20.750	1.100
21.750	.721
22.250	.320
22.750	.264
23.680	0

[a]The ordinates have been adjusted to correct the body areas for the cross-sectional area distribution of that part of the wing covered by this equivalent body.

Model Characteristics

Wing aspect ratio	2.096
Leading edge sweepback angle, deg	60.000
Trailing edge sweep angle, deg	-10.000
Free-stream airfoil of wing (Table II)	NACA 65A004
Total wing planform area, sq ft	5.050
Wing mean aerodynamic chord, ft	2.259
Fuselage fineness ratio	10.087
Fuselage frontal area, sq ft	0.194
Sweep angle of strut, deg	70.000
Free-stream airfoil of strut (Table III)	NACA 65A006
Total frontal area of Siamese nacelles, sq ft	0.136
Fineness ratio of one nacelle	8.900

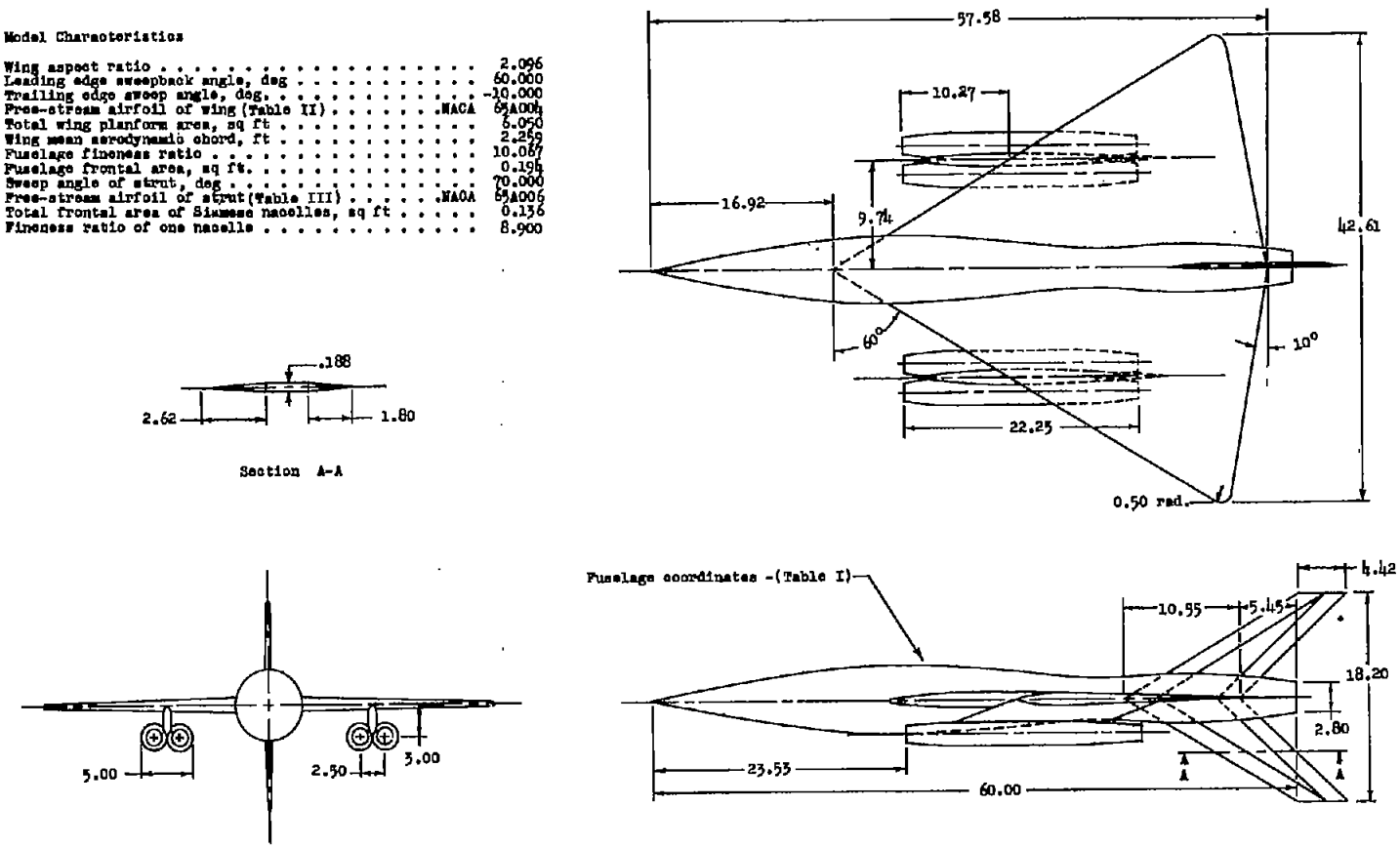

(a) Configurations with strut-mounted Siamese nacelles. Model A.

Figure 1.- Details and dimensions of models tested.

[redacted]

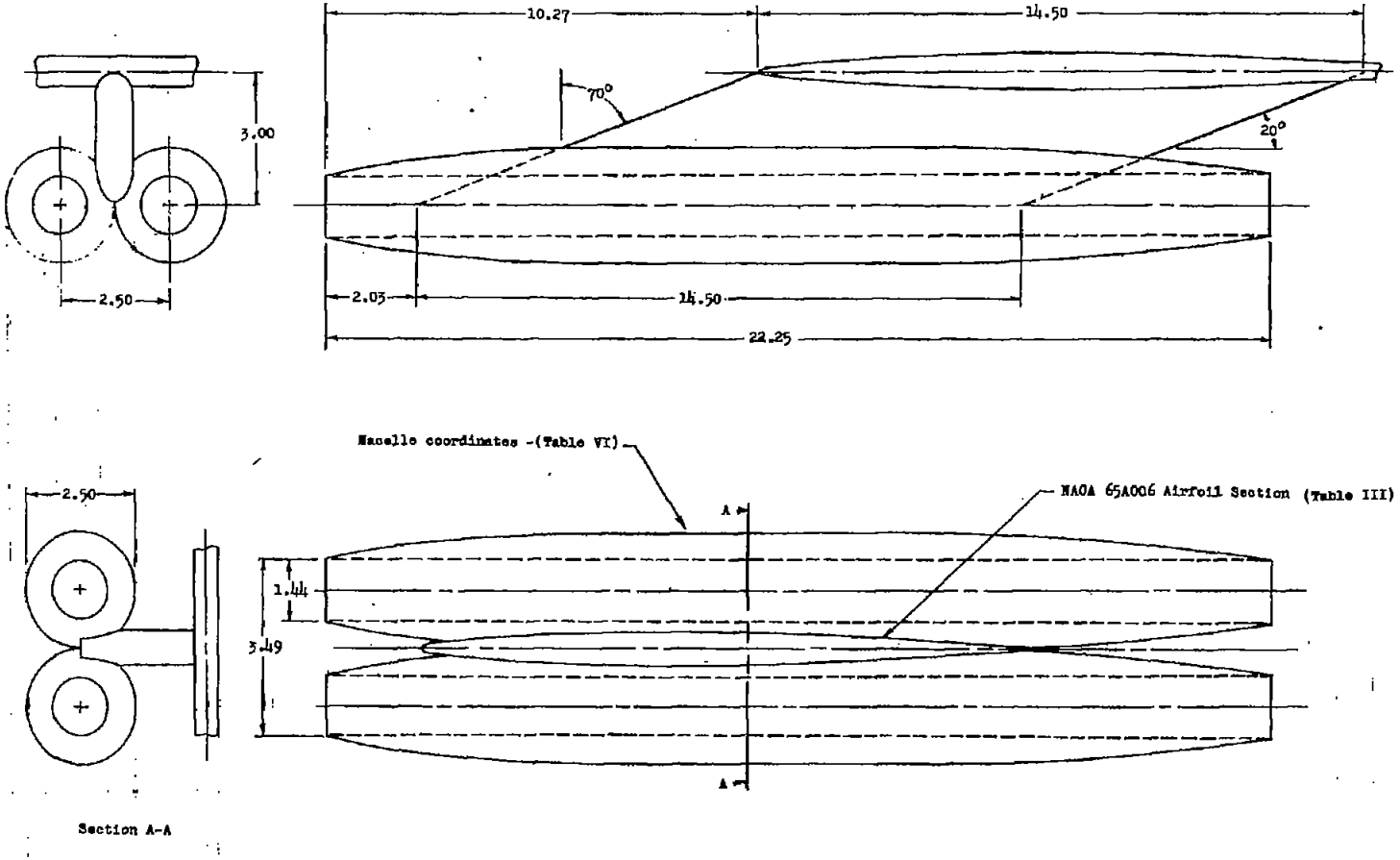

[redacted]

(b) Strut-mounted Siamese nacelles. Model A.

Figure 1.- Continued.

Model Characteristics

Wing aspect ratio	2.096
Leading edge sweepback angle, deg	60.000
Trailing edge sweep angle, deg.	-10.000
Free-stream airfoil of wing (Table II)	NACA 65A004
Total wing planform area, sq ft	6.050
Wing mean aerodynamic chord, ft	2.259
Fuselage frontal area, sq ft.	0.194
Fuselage fineness ratio	10.067

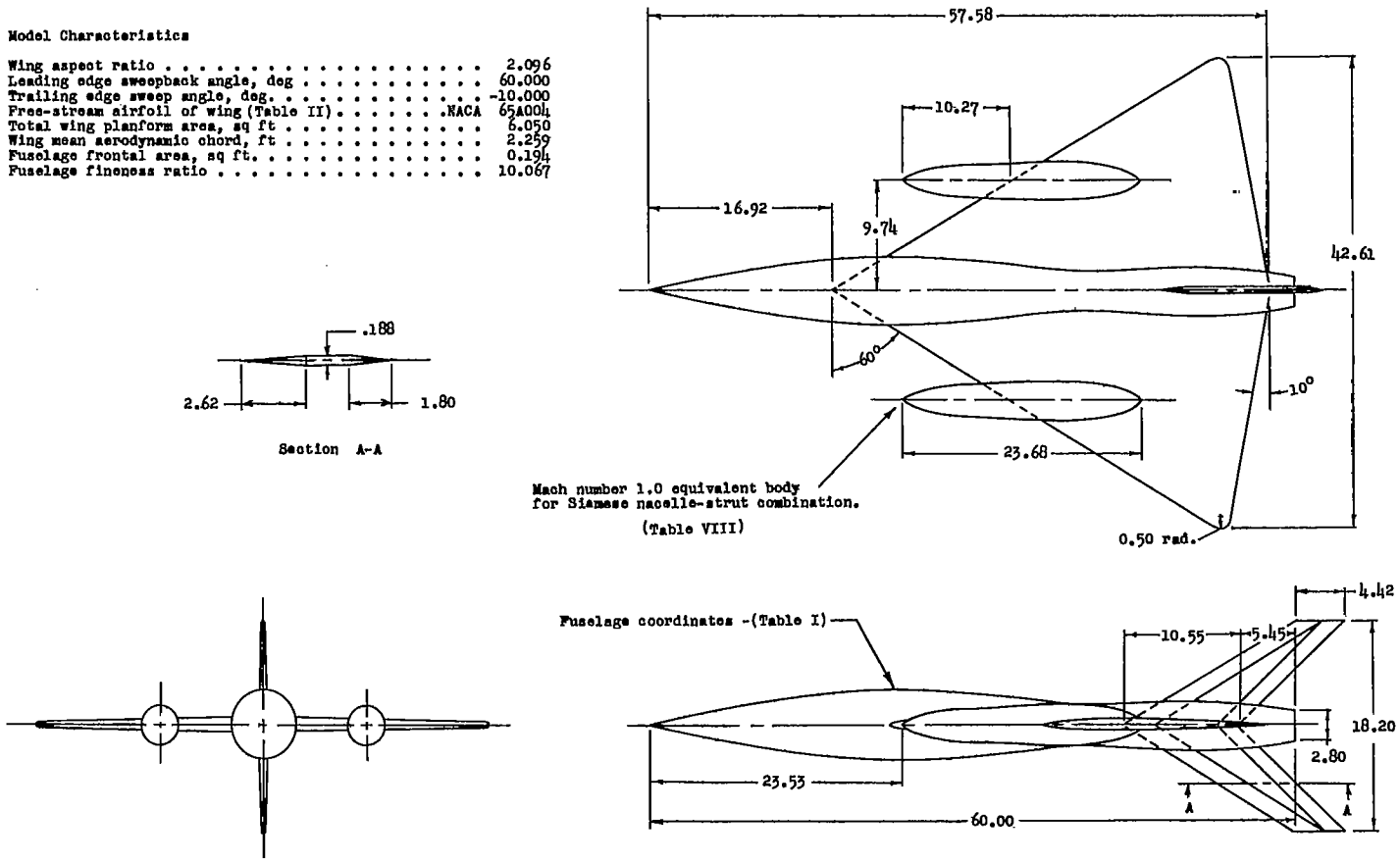

(c) Configuration with equivalent bodies for the struts and nacelles. Model B.

Figure 1.- Continued.

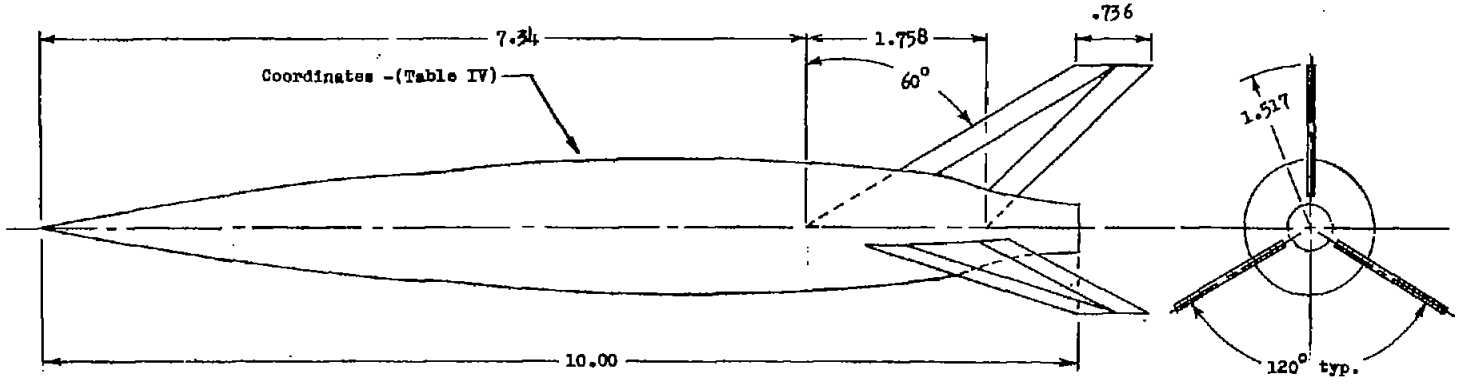

(d) Mach number 1.0 equivalent body for models A and B. Model C.

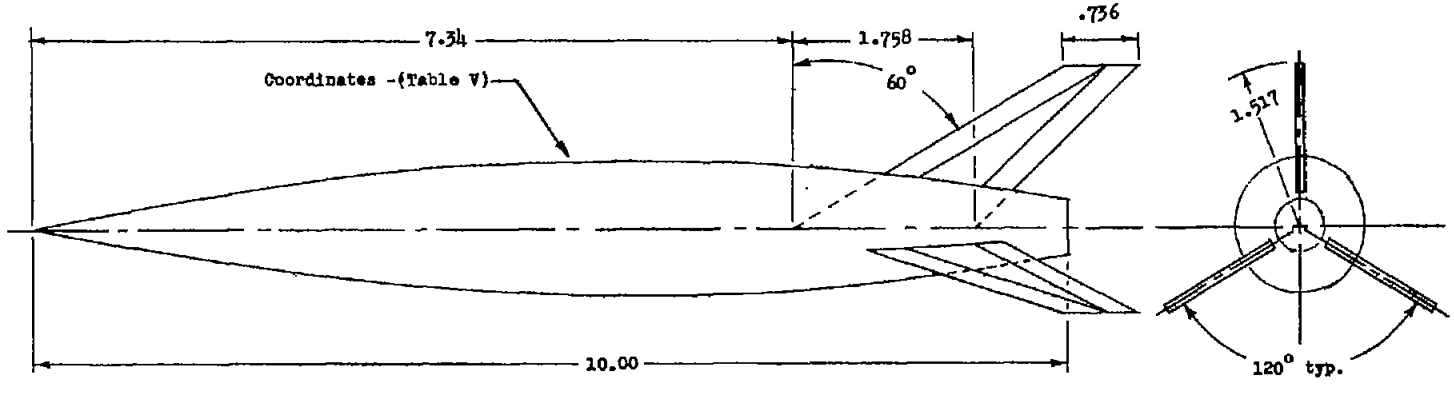

(e) Average equivalent body for models A and B at Mach number 1.2. Model D.

Figure 1.- Continued.

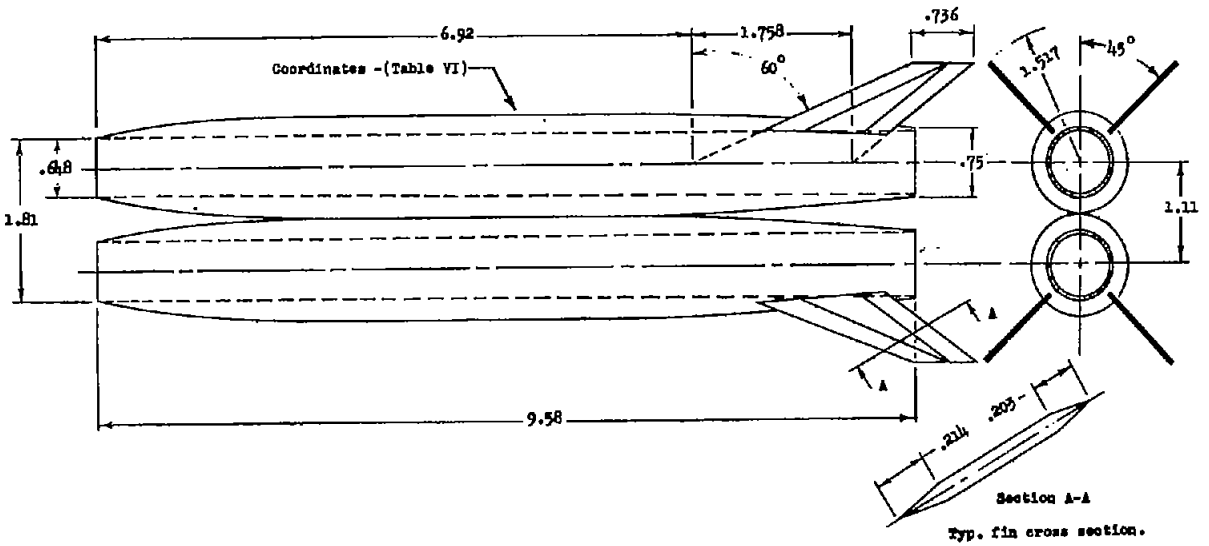

(f) Siamese nacelles. Models E and F.

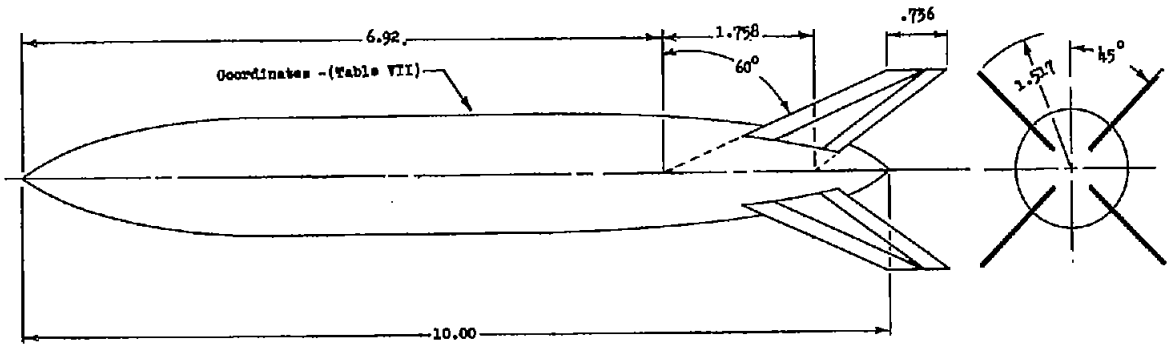

(g) Mach number 1.0 equivalent body for Siamese nacelles. Model G.

Figure 1.- Continued.

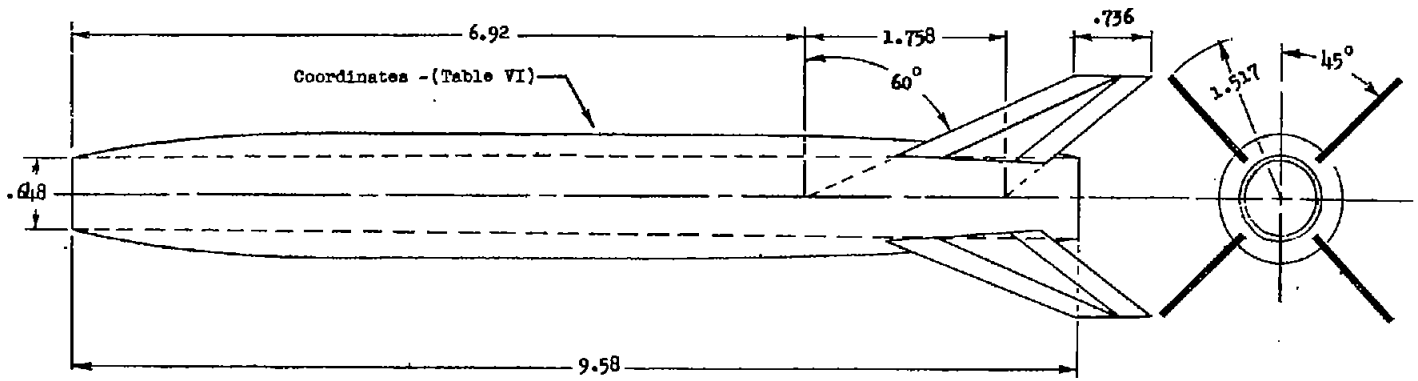

(h) Single nacelle. Model H.

Figure 1.- Concluded.

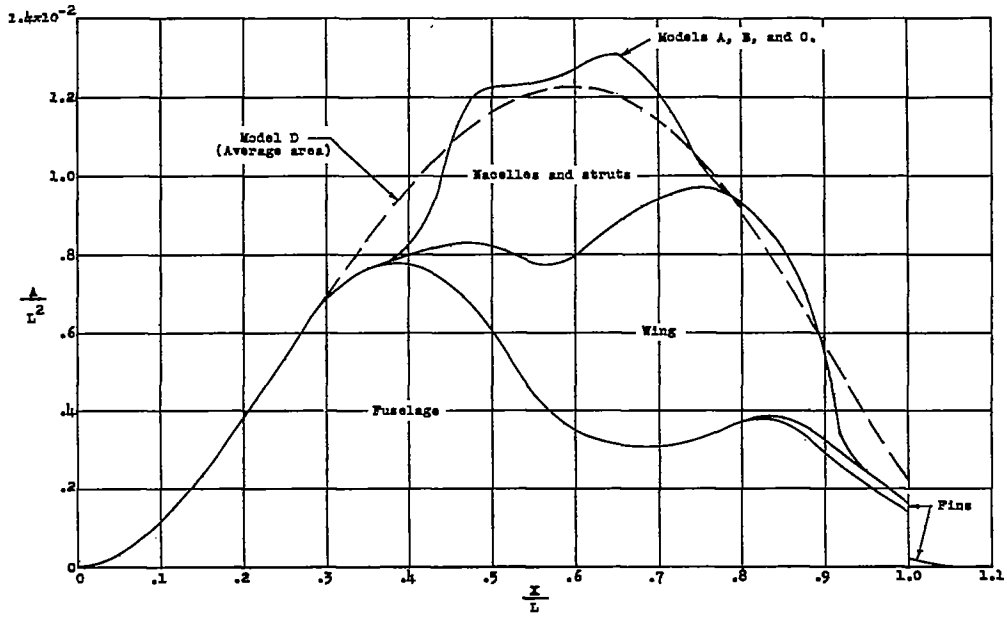

(a) Areas at Mach number 1.0.

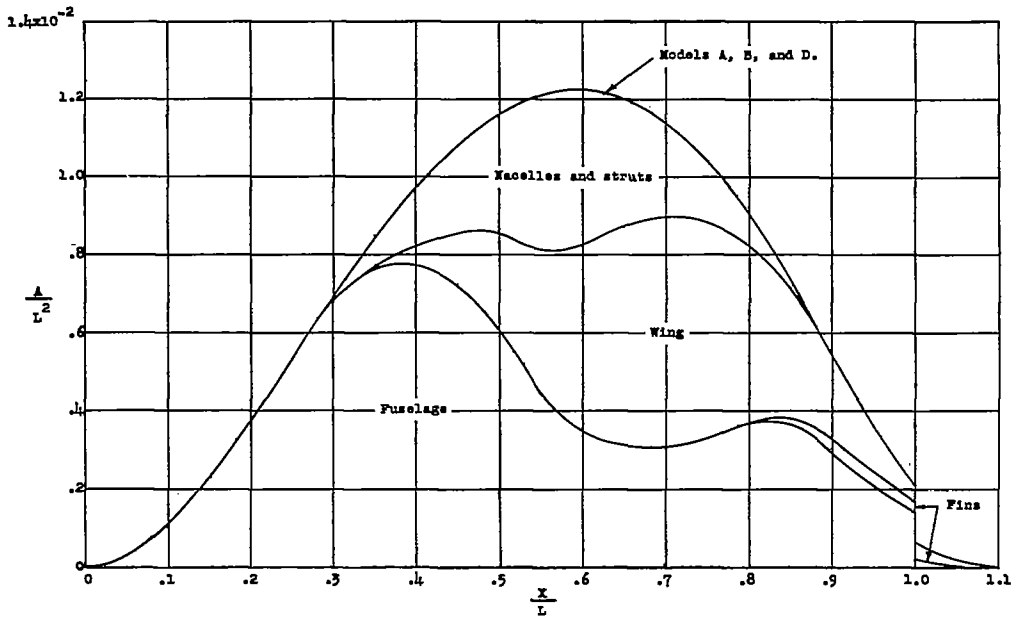

(b) Average areas at Mach number 1.2.

Figure 2.- Area distributions of models tested.

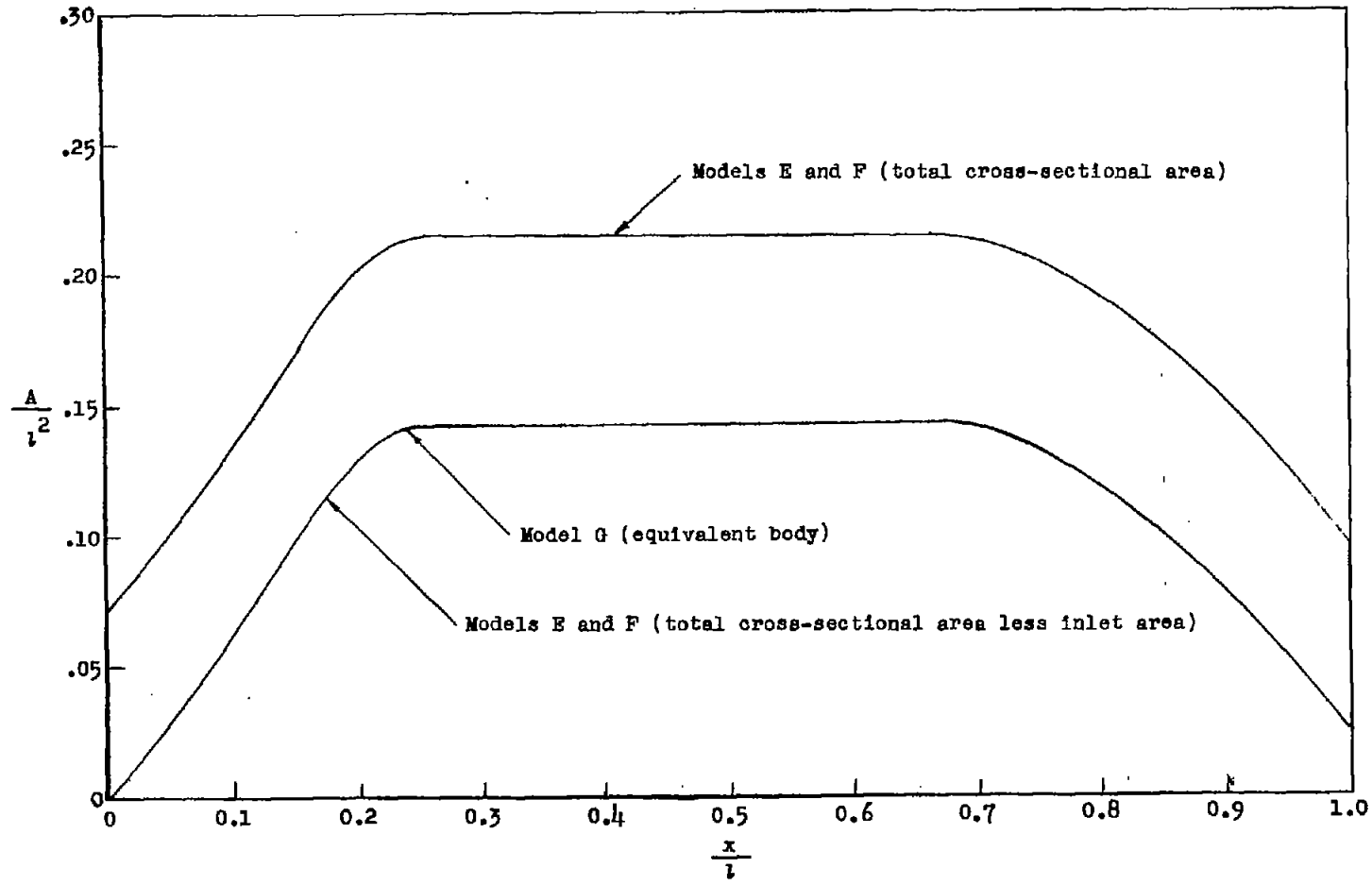

(c) Areas of Siamese nacelles at Mach number 1.0.

Figure 2.- Concluded.

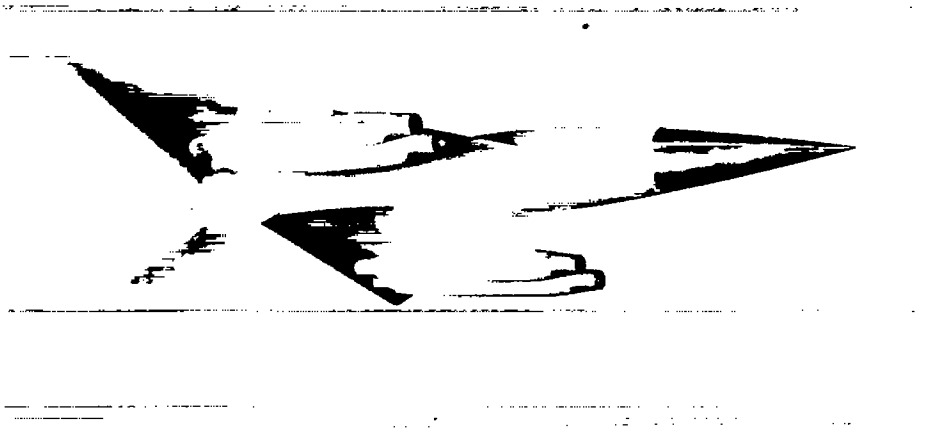

(a) Quarter-front view. Model A.

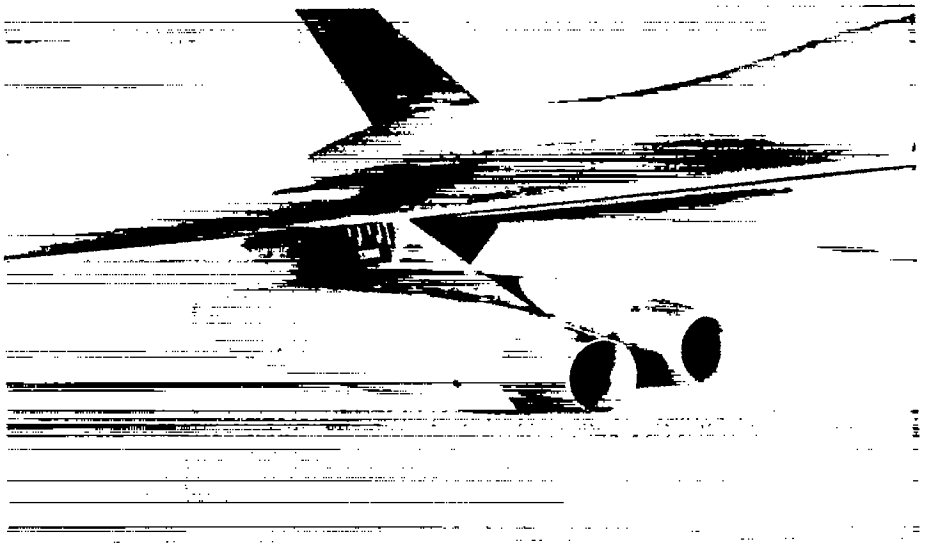

(b) Close-up of nacelle installation. Model A. L-57-2713

Figure 3.- Photographs of models.

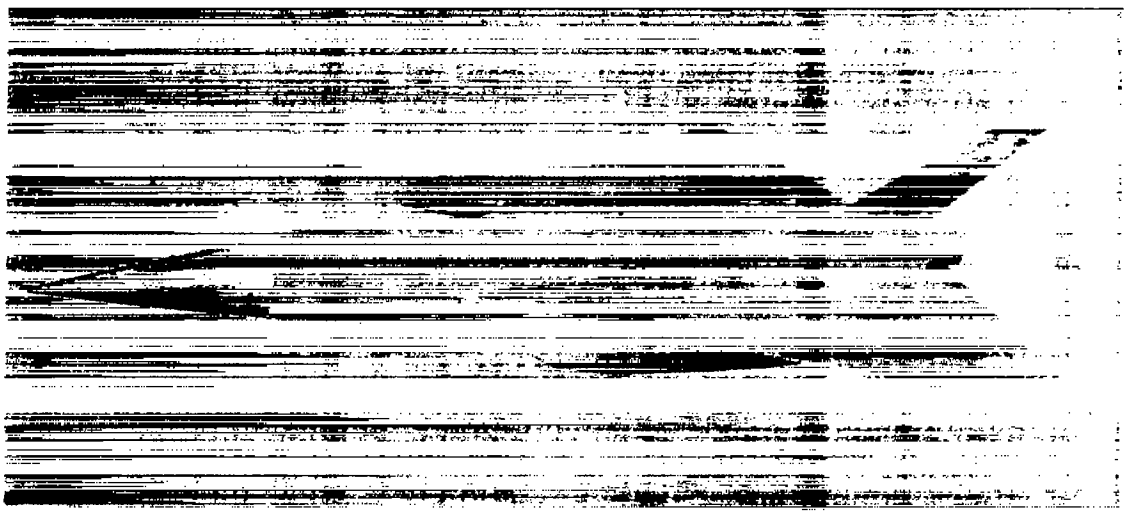

(c) Quarter-front view. Model B.

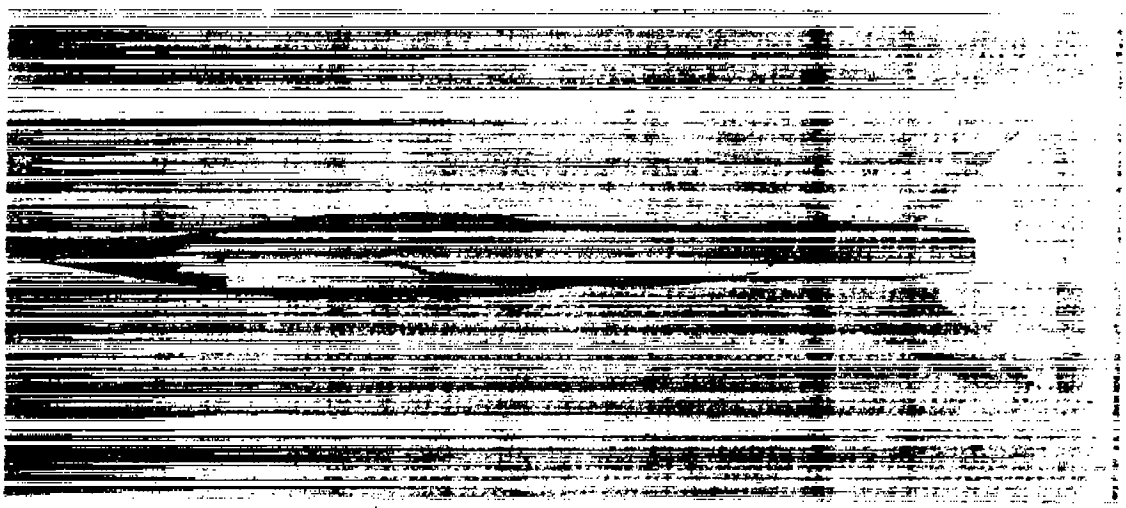

(d) Side view. Model B. L-57-2714

Figure 3.- Continued.

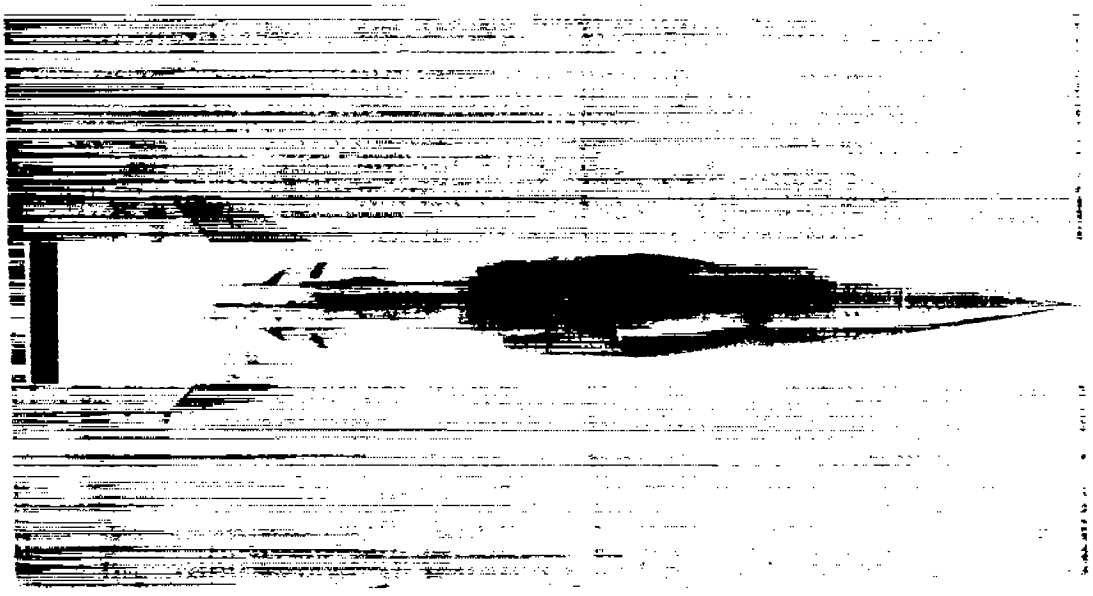

(e) Model C. L-84640

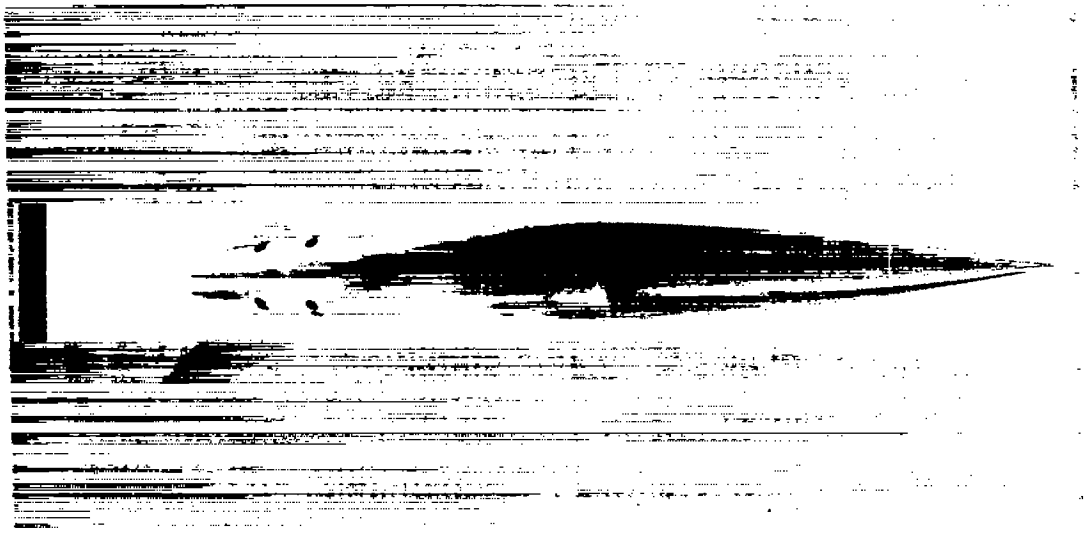

(f) Model D. L-84642

Figure 3.- Continued.

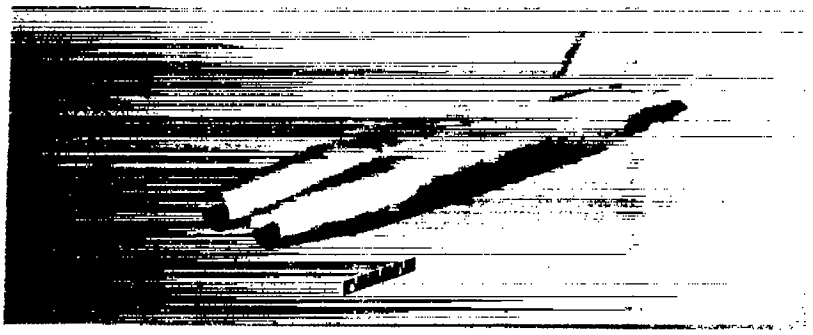

(g) Model E or F.

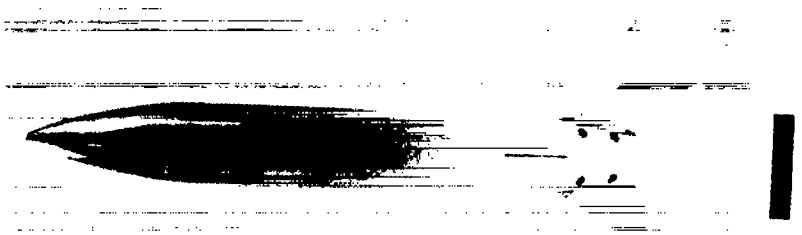

(h) Model G.

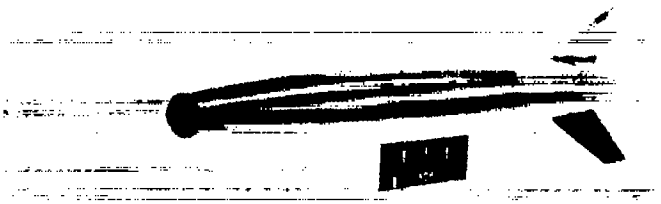

(i) Model H. L-57-2715

Figure 3.- Continued.

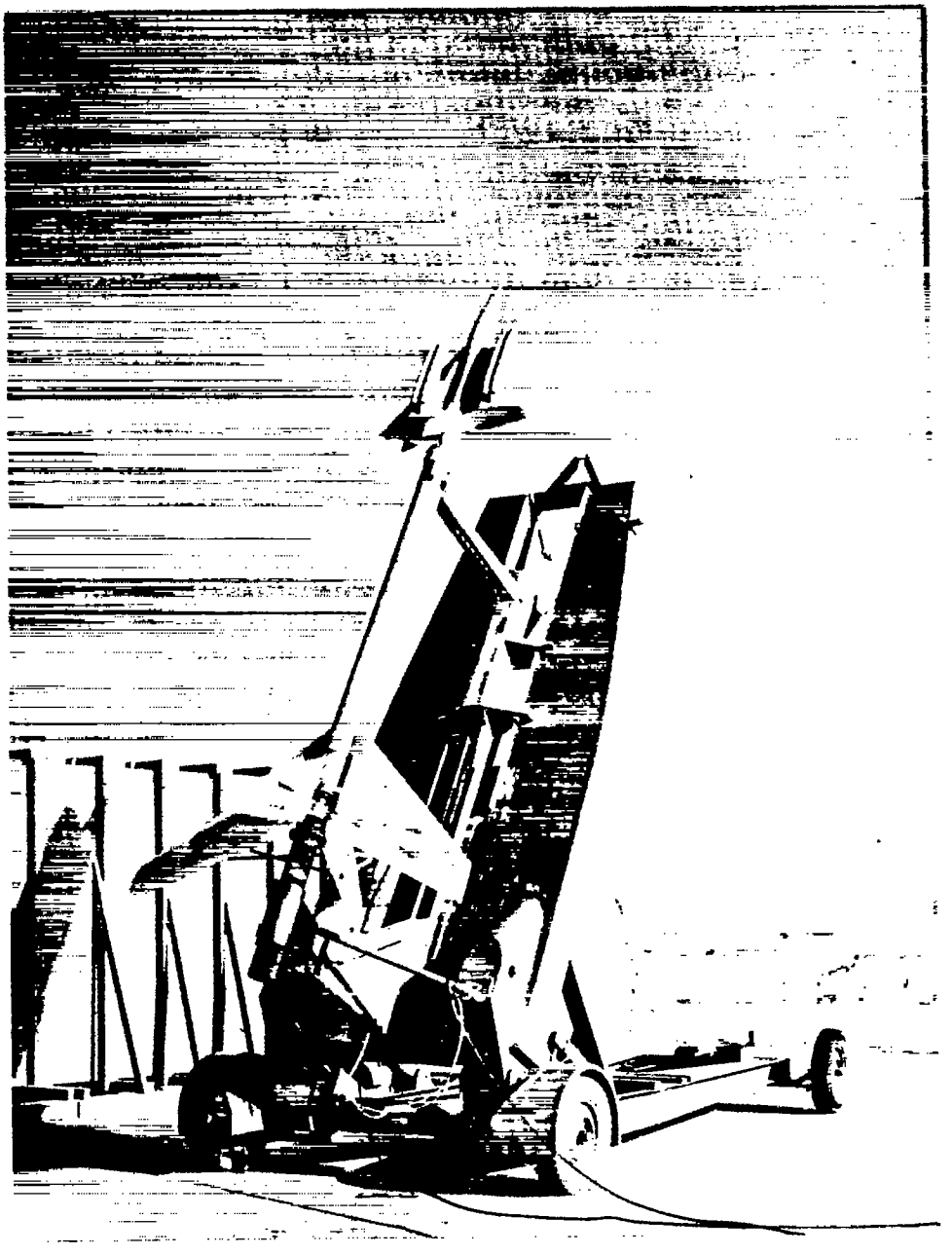

(j) Model A and booster on launcher. L-92636

Figure 3.- Concluded.

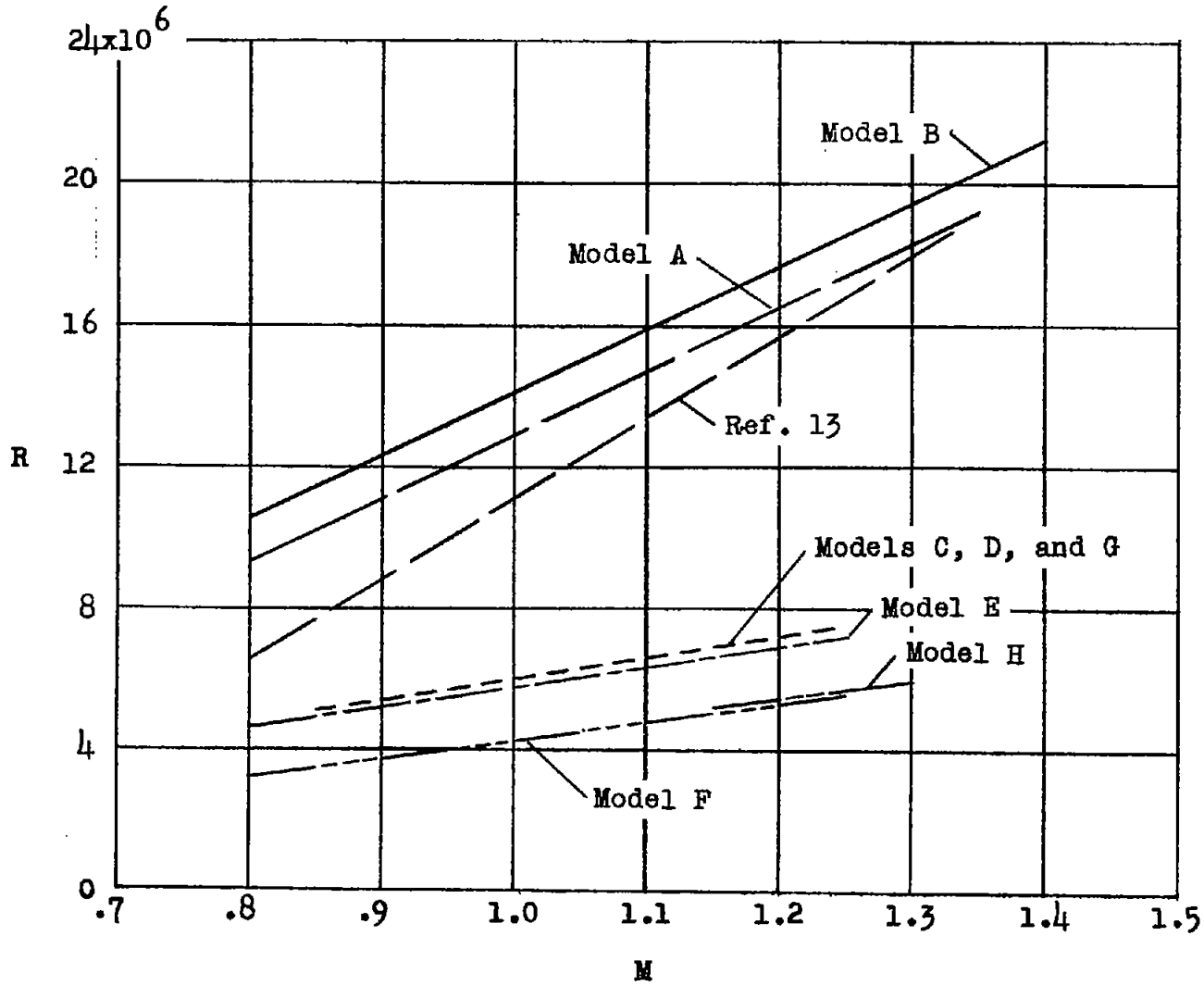

Figure 4.- Variations of Reynolds number with Mach number. Reynolds number based on mean aerodynamic chord adjusted for model scale.

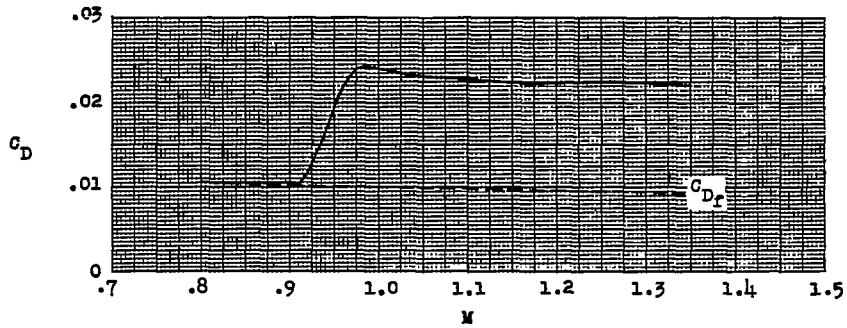

(a) Wing-body-struts-nacelles. Model A.

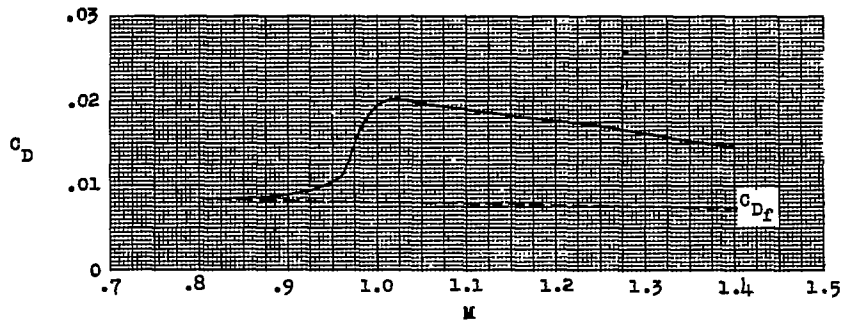

(b) Wing-body-equivalent struts and nacelles. Model B.

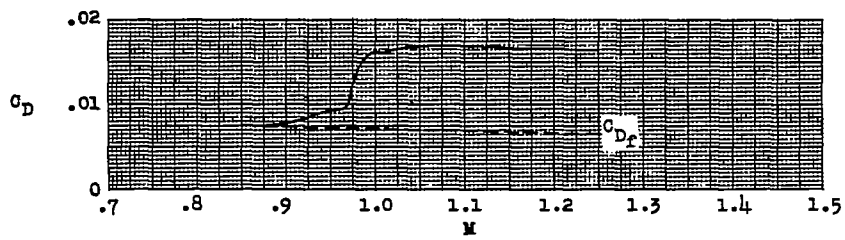

(c) Mach number 1.0 equivalent body. Model C.

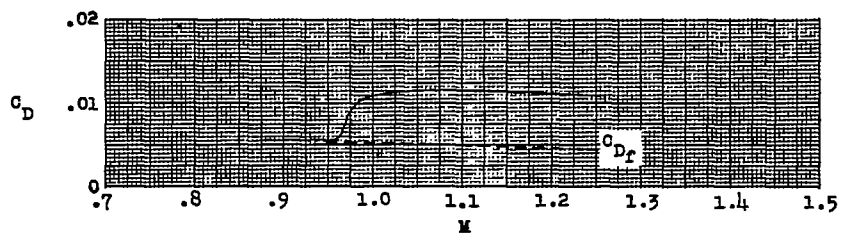

(d) Mach number 1.2 average equivalent body. Model D.

Figure 5.- Variations of total drag coefficient and friction drag coefficient with Mach number for the wing-body-nacelle configurations and their equivalent bodies of revolution.

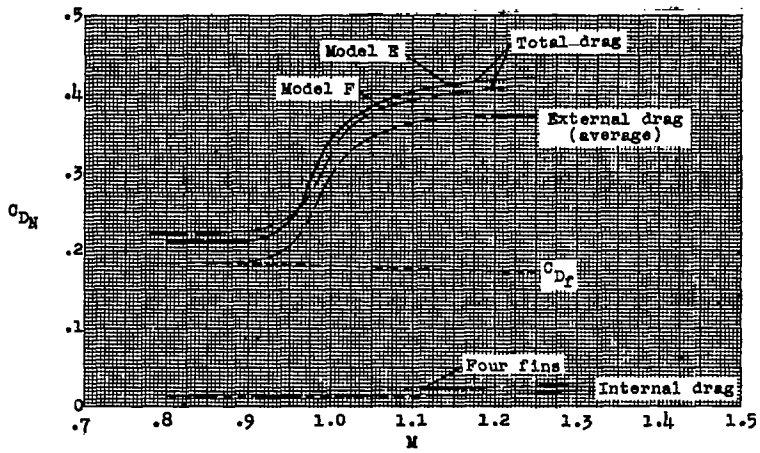

(a) Siamese nacelles. Models E and F.

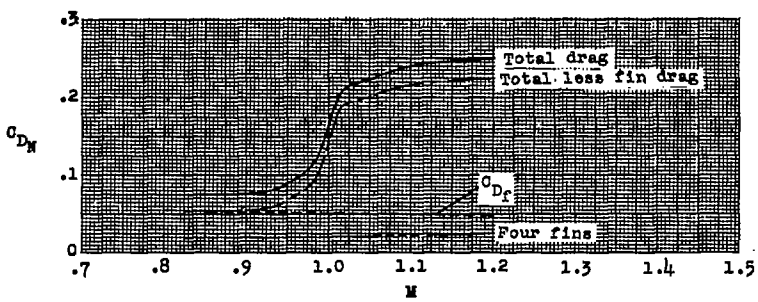

(b) Equivalent-body of Siamese nacelles. Model G.

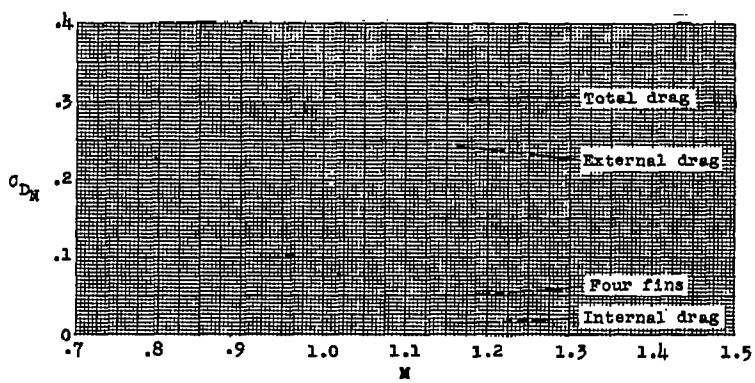

(c) Single nacelle. Model H.

Figure 6.- Variations of total drag, external drag, internal drag, fin drag, and friction drag coefficients with Mach number for the nacelle configurations tested.

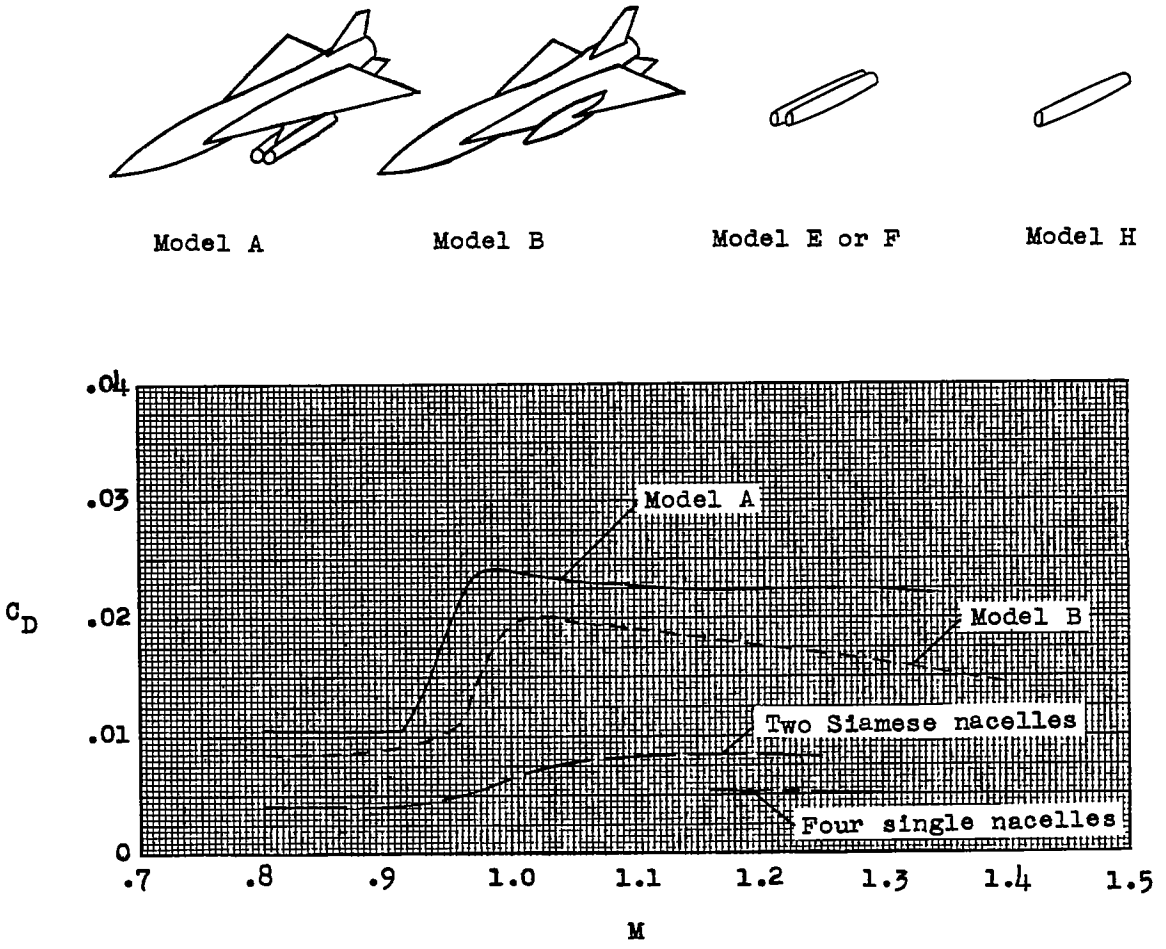

Figure 7.- Comparison of total drag coefficients of the wing-body-nacelle configurations and the external drag coefficients of the Siamese and single nacelles tested.

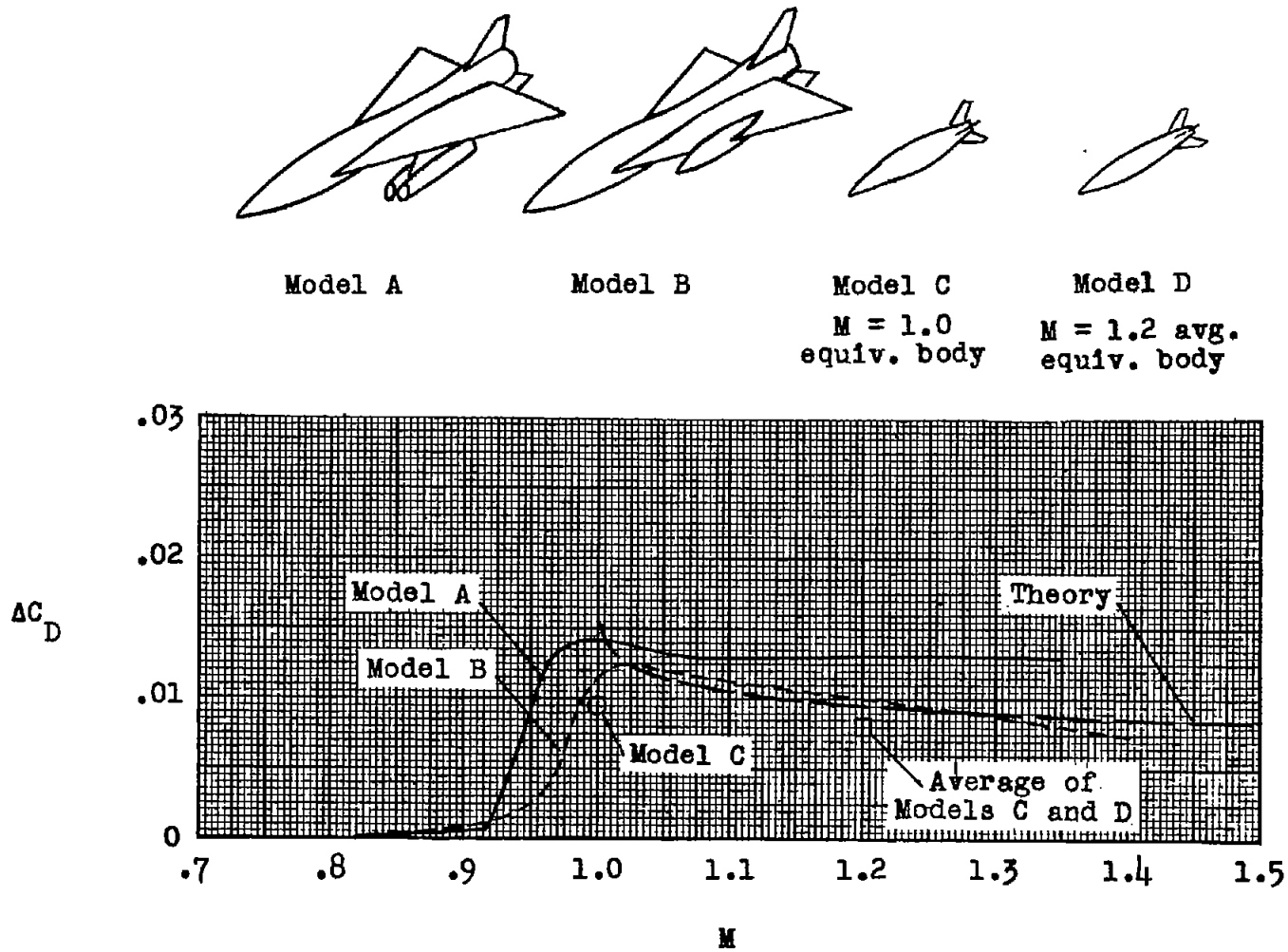

Figure 8.- Comparison of the drag rise of the wing-body-nacelle combinations with the theoretical pressure drag and the drag rise of the equivalent bodies of revolution.

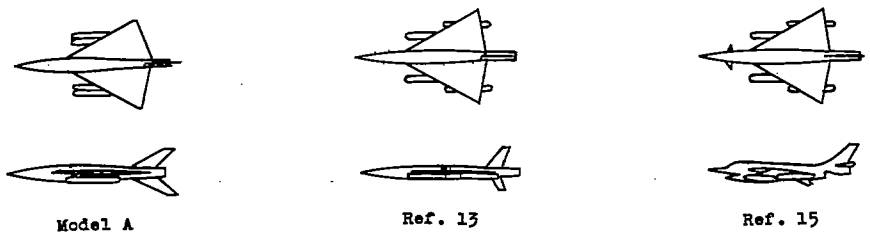

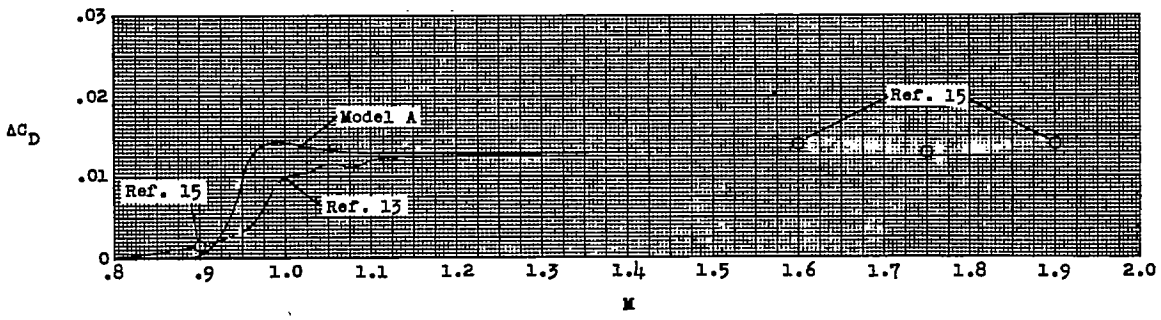

(a) Drag rise.

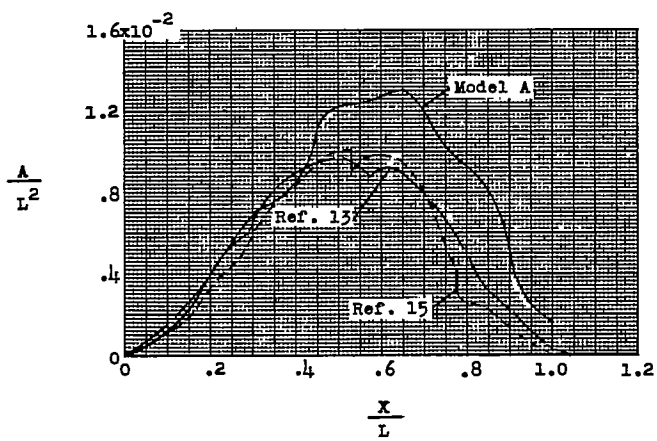

(b) Mach number 1.0 area distributions.

Figure 9.- Comparisons of the drag rise and normal cross-sectional area distributions of model A and two bomber configurations from references 13 and 15.

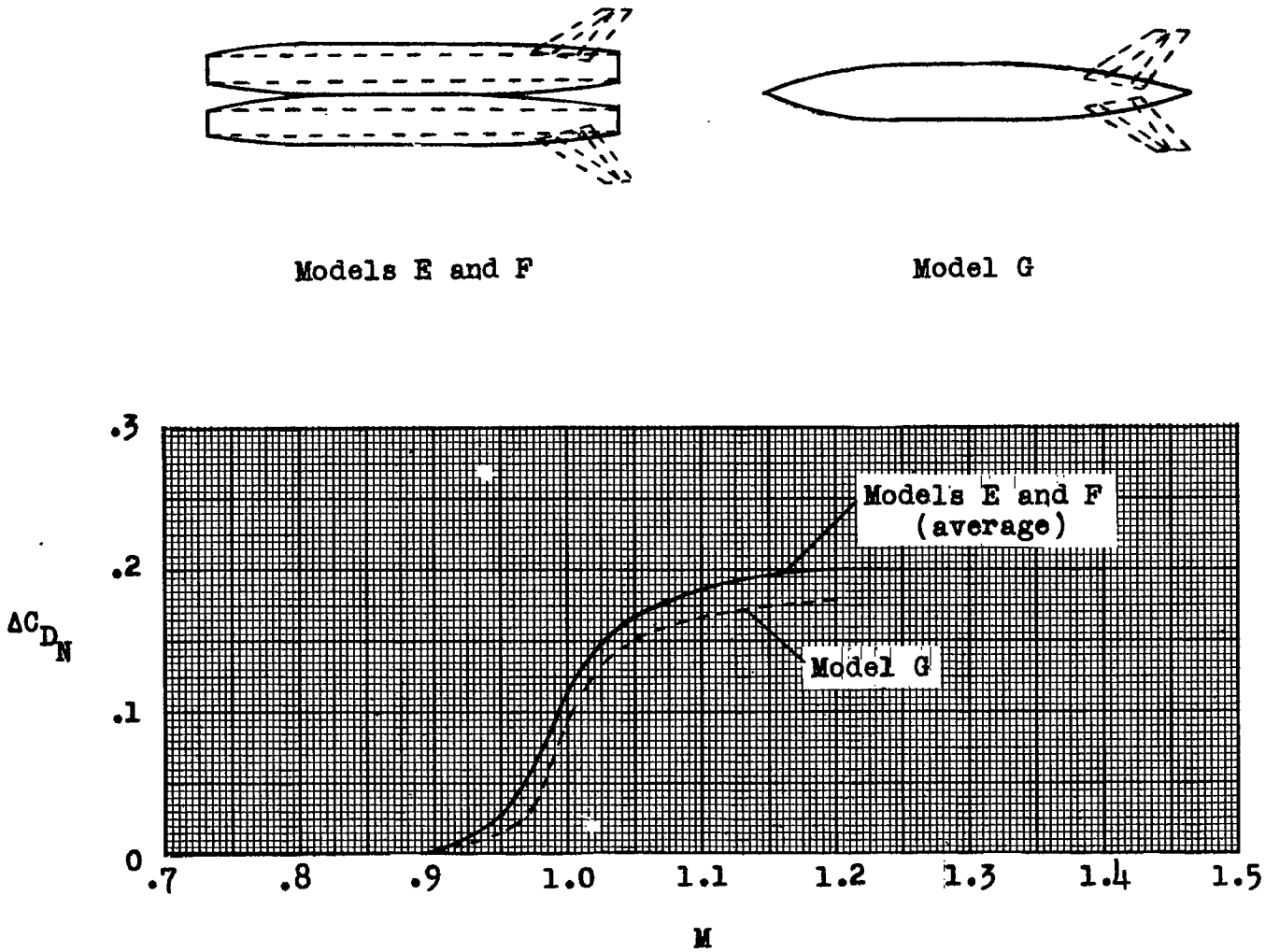

Figure 10.- Comparison of the external drag rise of the Siamese nacelles and the drag rise of the Mach number 1.0 equivalent body of revolution of the Siamese nacelles.